Supplementary Materials

Materials and Methods

Participants

For the Primary cohort and the Replication Cohort, children with ASD received an autism diagnosis based on scores from the Autism Diagnostic Interview-Revised (ADI-R) (Lord *et al.*, 2000) and/or the Autism Diagnostic Observation Schedule (ADOS) (Luyster *et al.*, 2009) following criteria established by the National Institute of Child Health & Human Development/National Institute of Deafness and Other Communication Disorders Collaborative Programs for Excellence in Autism (Lainhart, 2006). Children with ASD were screened through a parent phone interview and excluded if they had any history of known genetic, psychiatric, or neurological disorders (e.g., Fragile X syndrome or Tourette's syndrome), or were currently prescribed anti-psychotic medications. TD children were screened and excluded if they or a first-degree relative had developmental, language, learning, neurological, psychiatric disorders, or psychiatric medication usage, or if the child met the clinical criteria for a childhood disorder on the Child Symptom Inventory – Fourth Edition or Child and Adolescent Symptom Inventory. All participants underwent a battery of standardized neuropsychological assessments including WASI (Wechsler Intelligence Scale for Children–3rd Edition, Wechsler Intelligence Scale for Children–4th Edition, or Wechsler Abbreviated Scale of Intelligence (The Psychological, 1999)), and the Wechsler Individual Achievement Test (WIAT-II; Wechsler, 2001). Full Scale IQ was determined from scores on the WASI. The primary and the replication cohorts were part of

separate data collection efforts. Specifically, the primary cohort HARDI and fMRI data were obtained as part of a study investigating brain systems underlying social information processing in autism while the secondary cohort HARDI data were obtained as part of a study examining structural connectivity of large-scale brain networks in autism. Additionally, Primary and Replication cohort data were obtained from two different 3-Tesla GE Signa MRI scanners located in adjacent suites in the Stanford Richard M. Lucas Center for Imaging.

Primary Cohort

HARDI. Twenty-four children with ASD and twenty-four age-, gender-, and IQ-matched TD children were included in the HARDI part of this study. Children with ASD (23 males, 1 females) ranged in age from 8 to 13 years (mean age: 10.62) with an IQ range of 80 to 145 (mean IQ: 113.67), and TD children (24 males, 0 females) ranged in age from 8 to 13 years (mean age: 10.39) with an IQ range of 87 to 146 (mean IQ: 121.29) (Supplementary Table 1).

fMRI. Sixteen children with ASD and twenty age-, gender-, and IQ-matched TD children were included in the fMRI part of this study. All participants completed an fMRI task involving perception of social and non-social stimuli. Children with ASD (13 males, 3 females) ranged in age from 8 to 13 years (mean age: 10.82) with an IQ range of 83 to 139 (mean IQ: 119.23); the TD children (20 males, 0 females) ranged in age from 8 to 13 years (mean age: 10.46) with an IQ range of 87 to 146 (mean IQ: 126.06) (Supplementary Table 2, Supplementary Table 4). As noted below, AROMA (Pruim *et al.*, 2015) was used on fMRI data from each participant to correct for potential motion artefacts, and the two groups were matched on mean framewise

displacement, the six motion parameters and variance removed by AROMA (Supplementary Table 4).

Replication Cohort

HARDI. Seventeen children with ASD and seventeen age-, gender-, and IQ-matched TD children were included in the HARDI part of this study. Children with ASD (15 males, 2 females) ranged in age from 8 to 13 years (mean age: 10.60) with an IQ range of 85 to 150 (mean IQ: 107.59); the TD children (15 males, 2 females) ranged in age from 8 to 13 years (mean age: 10.57) with an IQ range of 93 to 136 (mean IQ: 116.82) (Supplementary Table 1).

Imaging

Structural MRI

Structural MRI acquisition

A high resolution T1-weighted spoiled gradient recalled (SPGR) inversion recovery 3D MRI sequence was acquired for selecting the regions of interest. The following parameters were used: TI = 400 ms, TR = 5.9 ms; TE = 1.952 ms; flip angle = 11^{o} ; 22 cm field of view; 166 slices in axial plane; 256 × 192 matrix; 2 NEX, acquired resolution = 0.9375 × 0.9375 × 1.0 mm

Structural MRI Processing

MR images were processed with *FreeSurfer* (http://surfer.nmr.mgh.harvard.edu, v5.3) to obtain the NAc segmentation for each subject in their native space (Fischl *et al.*, 2002). Prior to cortical reconstruction, all images were resampled to a common isotropic voxel size of 1x1x1mm.

To facilitate ROI generation for functional analyses, the MNI template T1w volume was co-registered individual T1w images using ANTs. The registration procedure comprised four stages each of rigid and affine co-registrations (# iterations = 10000, 10000, 11110, 11110, shrink factors = 8, 4, 2, 1, smoothing sigmas = 4, 3, 2, 1) using the NMI cost metric, followed by three stages of SyN (# iterations = 100, 30, 20, shrink factors = 8, 4, 2, smoothing sigmas = 4, 2, 1) using NMI and CC as the cost metrics.

HARDI

HARDI acquisition

The HARDI pulse sequence was a diffusion-weighted single-shot spin-echo, echo planar imaging sequence (TE = minimum; TR = 5.3 s; field of view = 260 mm; matrix size = 128 × 128; bandwidth = ±250kHz; partial k-space acquisition). The following parameters were used: 50 axial, 2.9-mm thick slices (no skip) for 2 b values, b = 0 and b = approximately 2500 s/mm^{2}The high b value was obtained by applying gradients along 150 different diffusion directions.

HARDI preprocessing

HARDI data were preprocessed to simultaneously correct for head motion and eddy-current-induced distortions using the method developed by Rohde et al. implemented in mrDiffusion (Rohde *et al.*, 2004), and resampled to 2mm isotrophic voxels using a spline-based interpolation. Our acquisition does not include the blip up/down (reverse phase encoded) acquisitions necessary to perform susceptibility distortion correction (i.e. TOPUP). The diffusion gradient vectors were rotated to preserve their orientation with respect to anatomy. Response functions

(RFs), which are used as kernel during the constrained spherical deconvolution (CSD) step, for each participant were estimated using the "Tournier" algorithm with default parameters in MRtrix3's *dwi2response*. CSD was then performed using the computed RFs to estimate fiber orientation distribution functions (fODFs) with a maximum spherical harmonic degree of ten (Tournier *et al.*, 2012).

HARDI quality control

Systematic differences in HARDI data quality can lead to spurious findings across groups particularly when comparing children with ASD, who may be more prone to head motion during acquisition, to their typically developing peers (Koldewyn *et al.*, 2014; Yendiki *et al.*, 2014). Subjects with extreme excessive motion were excluded, and we used the approach of Yendiki and colleagues (Benner *et al.*, 2011; Koldewyn *et al.*, 2014), to quantify data quality and match across the two groups. Specifically, we computed four measures of HARDI data quality: (1) average translation, (2) average rotation, (3) percent bad slices, and (4) average dropout score (Supplementary Table 3). Importantly, TD and ASD groups did not differ significantly in any of the four measures, in both cohorts.

HARDI ROI selection

ROIs for the NAc and Amygdala were extracted from the FreeSurfer-based segmentation of each individual's T1-weighted image. To transform these ROIs to diffusion space, we first performed co-registration of the T1 and FA images, using ANTs. The registration procedure comprised four stages of rigid alignment (# iterations = 1000, 500, 250, 100, shrink factors = 8, 4, 2, 1, smoothing sigmas = 3, 2, 1, 0) followed by three stages of Symmetric Normalization (# iterations

= 100, 50, 30, shrink factors = 3, 2, 1, smoothing sigmas = 2, 1, 0), each using NMI as the cost metric. Next, the T1-space NAc and Amygdala ROIs were warped to diffusion space using the inverse of the transformations derived from the co-registration of the FA and T1 images described above. A white matter mask was also extracted and warped to diffusion space using the same transformations. NAc and Amygdala ROIs were then dilated once into the white matter to ensure feasibility of tractography.

ROIs for the VTA were generated in MNI space from midbrain peaks in the "REWARD" (Delgado *et al.*, 2000) contrast z-map distributed in the R440 data released as part of the Human Connectome Project (Van Essen *et al.*, 2012). This approach allowed us to reliably identify VTA voxels that are most sensitive to reward. The z-map was rotated to bring the midbrain section containing the VTA into the plane of image, inclusively masked using a 2D MNI-template transform. The transform was generated as follows: First, we delineated the midbrain section containing the VTA. by reorienting the entire brain volume to obtain an axial section encompassing the mammillary body and the superior colliculi following previously suggested procedures (Eapen *et al.*, 2011). Then, we used a region growing approach to segment the midbrain from non-midbrain structures. The same procedure was also applied to the Montreal Neurological Institute (MNI) template brain to create a normalized reference space for the midbrain sections. The resulting template was thresholded at the level z >= 6, masked to exclude posterior voxels (y < −20mm), symmetrized by reflecting across the Z-Y plane, and binarized. Each participant's midbrain section was co-registered to that of the MNI template using Advanced Normalization Tools (ANTs) (Avants *et al.*, 2011). Separate registrations were carried out in 2D for each slice, optimizing parameters for a set of linear transformations (translation,

rigid, affine) followed by a nonlinear transformation (Symmetric Normalization [SyN]). For each linear transformation, three stages were performed with numbers of iterations = 100000, 111100, 111100, shrink factors = 3, 2, 1, and smoothing sigmas = 4, 2, 1, respectively, and normalized mutual information (NMI) as the cost metric. SyN was carried out in three stages using number of iterations = 100, 30, 20, shrink factors = 4, 2, 1, and smoothing sigmas = 1, 0.5, 0, respectively, and a combined cost metric comprising NMI and CC. Finally, to project the ROIs to individual subject HARDI space, ROIs were first warped to the space of each subject's midbrain section using the inverse parameters from the co-registration to the 2D MNI midbrain section. These 2D ROIs were placed in the space of the (3D) reoriented T1w images described above, then projected to HARDI space by prepending the linear transformation (derived from rotating the T1 to place the midbrain section in the plane of the image) to the T1-to-FA transformations.

HARDI Tract analysis

Probabilistic tractography was performed by seeding 10,000 points in each voxel of an ROI and generating streamlines using the iFOD2 algorithm (Tournier JDC and Connely, 2010) in MRtrix3. iFOD2 is an improved probabilistic streamlines tractography by 2nd order integration over fibre orientation distributions. iFOD2 is also the recommended approach in Mrtrix3. In our case, we iFOD2 with the following default parameters: step size = 0.5*voxel size = 1mm, angle = 90deg * step size / voxel size = 90deg * 1mm / 2mm = 45 deg, FOD amplitude cutoff = 0.1. All valid streamlines, according to MRTrix3 criteria, were included in subsequent analyses. Fiber density – the source- and target-volume-normalized fraction of streamlines emanating from the seed ROI and intersecting the ipsilateral target ROI – was then computed for each child and

used as a measure of structural integrity. In separate analyses, the NAc was seeded and targets in the VTA and Amygdala were used to measure NAc-VTA and NAc-Amygdala fiber densities, respectively. These fiber density values were compared between the two groups.

Relationship between structural connectivity and ASD symptom severity: Multivariate analysis

We used multivariate sparse regression (LASSO) combined with cross-validation analysis (Tibshirani, 1996) to determine the relationships between the structural connectivity and the ASD symptom severity. Our machine learning approach overcomes several shortcomings of conventional linear regression methods: The LASSO regression algorithm produces more interpretable solutions as it employs the L1 regularization procedure that drives the small magnitude coefficients/weights to zero thereby performing automatic feature selection. This regularization procedure also prevents over-fitting of the data and therefore improves the generalizability of the regression model. The use of cross-validation further prevents over-fitting.

ADI-R Social Interaction subscale score, ADI-R Communication and Language subscale score, ADI-R Restricted and Repetitive Behaviors subscale score, age, and IQ as independent variables and NAc-VTA fiber density as dependent variable were used as the input to a LASSO regression algorithm. Leave-one-out-cross-validation (LOOCV) procedure was used to select the L1 regularization tuning parameter lambda. In LOOCV, data are divided into N folds (where N is the number of subjects). LASSO regression models for a range of lambda values are built using N – 1 folds, leaving out one sample. The left out sample is then used as a validation set for these regression models. The above procedure is repeated N times by leaving out one sample each

time, and finally an optimal lambda is selected. For the optimal lambda value, beta coefficient and the associated *P* value for each independent variable is then computed. The aforementioned procedures were implemented using the R packages glmnet[1] and selectiveInference[2].

fMRI

fMRI acquisition

A total of 31 axial slices (4.0mm thickness, 0.5mm skip) parallel to the ACPC line and covering the whole brain were imaged using a T2*-weighted gradient echo spiral in-out pulse sequence (Glover and Law, 2001) with the following parameters: TR = 2000 ms, TE = 30 ms, flip angle = 80°, 1 interleave, for the duration of a 4-minute task scan. Head movement was minimized during scanning by small cushions.

fMRI preprocessing

A linear shim correction was applied separately for each slice during reconstruction using a magnetic field map acquired automatically by the pulse sequence at the beginning of the scan. Functional MRI data were then analyzed using SPM8 analysis software (http://www.fil.ion.ucl.ac.uk/spm). Images were realigned to correct for motion, corrected for errors in slice-timing, spatially transformed to standard stereotaxic space (based on the Montreal Neurologic Institute (MNI) coordinate system), resampled every 2 mm using sinc interpolation and smoothed with a 6mm full-width half-maximum Gaussian kernel to increase the signal-to noise ratio prior to statistical analysis. Translational movement in millimeters (x, y, and z) and rotational motion in degrees (pitch, roll, and yaw) were calculated based on the SPM parameters

[1] https://cran.r-project.org/web/packages/glmnet/index.html
[2] https://cran.r-project.org/web/packages/selectiveInference/index.html

for motion correction of the functional images in each subject. Motion correction was performed on the smoothed images, using an Independent Component Analysis (ICA) – based AROMA method, using procedures described in (Pruim *et al.*, 2015).

fMRI regions of interest (ROI) selection

Regions of interest for the VTA were generated from the midbrain peaks in the "REWARD" (Delgado *et al.*, 2000) contrast z-map distributed in the R440 data released as part of the Human Connectome Project, using procedures described above. Regions of interest for the NAc and Amygdala were generated by inverting and applying the MNI to T1 transforms (described in the Section: T1-weighted MRI Processing) to the subject-space NAc and Amygdala ROIs, averaging across subjects and thresholding at 0.5 to create a probabilistic group-consensus MNI-space NAc and Amygdala ROI.

fMRI Signal-to-Noise Ratio (SNR) analysis

We computed SNR of the fMRI signal in each of the ROIs – NAc, VTA, Amygdala and compared the computed SNR values between the ASD and TD groups using two sample t-tests. SNR of the fMRI signal in a ROI was calculated as the ratio of mean of the ROI fMRI timeseries and standard deviation of the ROI fMRI timeseries.

fMRI connectivity analysis

The regional fMRI timeseries was computed for each of the ROIs – NAc, VTA, Amygdala – by computing the first eigenvector of timeseries of all the voxels within each region. We examined the functional connectivity between the regions of interest using the generalized

psychophysiological interaction (gPPI) model (McLaren *et al.*, 2012), with the goal of identifying connectivity between the NAc and VTA in response to social (face) and non-social (scene) stimuli. We used SPM gPPI toolbox for this analysis. gPPI is a method that is more sensitive than PPI to context-dependent differences in the connectivity (McLaren *et al.*, 2012). Unlike dynamical causal modeling (DCM), gPPI does not use a temporal precedence model (x(t+ 1) ~ x(t)) and therefore makes no claims of causality. At the individual subject level, the regional timeseries from each ROI is deconvolved to uncover neuronal activity and then multiplied with the task design waveforms to form an interaction term. This interaction term is then convolved with the hemodynamic response function (HRF) to form the gPPI regressor, and the resulting timeseries of one ROI is regressed against the other two ROIs. This final step is repeated for each ROI yielding functional connectivity values between the NAc and the VTA, and the NAc and the Amygdala, in response to face and scene stimuli respectively. The aforementioned model is summarized in Equation 1 and Equation 2.

$$VTA \sim NAC + conv\big(deconv(NAc) * task_{waveform}\big) \quad (1)$$

and similarly,

$$Amygdala \sim NAC + conv\big(deconv(NAc) * task_{waveform}\big) \quad (2)$$

Given our goal of contrasting differential functional connectivity responses to social vs. non-social stimuli, we performed between group t-tests on the differences between the computed functional connectivity values for faces and scenes.

Relationship between functional connectivity and ASD symptom severity: Multivariate analysis

We repeated the multivariate sparse regression combined with cross-validation analysis with strength of functional interactions between the NAc and VTA in response to social stimuli as dependent variable, and ADI-R Social Interaction subscale score, ADI-R Communication and Language subscale score, ADI-R Restricted and Repetitive Behaviors subscale score, age, and IQ as independent variables.

Results

Robustness of functional connectivity findings against potential motion-related confounds

In light of recent concerns about the influence of head motion on functional connectivity estimates, we applied a stringent movement exclusion criterion, as recently recommended by Fornito and colleagues (Parkes *et al.*, 2017), and repeated the functional connectivity analyses. Specifically, we excluded participants who have mean framewise displacement greater than 0.55. Additionally, we matched the two groups on mean framewise displacement and six other motion parameters, and age resulting in a sample consisting of thirteen children with ASD and well-matched thirteen TD children (Supplementary Table 4). The results from this analysis were similar to the original results: (i) children with ASD, in contrast to their TD peers, showed decreased functional connectivity between the NAc and VTA during face processing relative to scene processing ($M_{ASD} = -0.46$, $SD_{ASD} = 0.60$, $M_{TD} = 0.16$, $SD_{TD} = 0.85$, $t(24) = -2.16$, $P = 0.04$, Bayes Factor (BF) = 1.88, *Cohen's d* = −0.85, Supplementary Fig. 2), (ii) no significant

group differences in functional connectivity between the NAc and the Amygdala during face relative to scene processing (M_{ASD} = −0.09, SD_{ASD} = 0.77, M_{TD} = −0.02, SD_{TD} = 0.85, $t(24)$ = −0.21, P = 0.84, Bayes Factor (BF) = 0.37, *Cohen's d* = −0.08), and (iii) in children with ASD, the ADI-R Social Interaction subscale scores and not the ADI-R Communication and Language or the ADI-R Restricted and Repetitive Behaviors subscale scores, were uniquely associated with NAc-VTA functional connectivity (Supplementary Table 8).

Relationship between structural/functional connectivity of the mesolimbic reward pathway and social interaction impairments, as measured by ADOS

We performed analysis to determine the relationship between social interaction impairments as measured by ADOS and the structural connectivity and the functional connectivity of the reward pathway. We did not find a significant relationship between the severity of social impairments as measured by ADOS social interaction subscale, and (i) the density of the NAc-VTA tracts (Primary Cohort: r_s (20) = −0.31, P = 0.18, BF = 0.78; Replication Cohort: $r_s(15)$ = −0.21, P = 0.45, BF = 0.54), and (ii) the strength of functional interactions between the NAc and VTA in response to social stimuli, in children with ASD ($r_s(16)$ = 0.05, P = 0.86, BF = 0.43).

fMRI SNR analysis

In light of concerns that VTA is an area that can be hard to reliably collect fMRI data, we performed SNR analysis and found no significant between group differences in the SNR values of the three ROIs in the TD group (F(2, 57) = 1.31, P = 0.28) and in the ASD group (F(2, 45) = 1.04, P = 0.36).

Figures

Figure 1. **Control analyses based on NAc-Amygdala tracts.** (**A-C**) Using analytical procedures illustrated in main Fig. 1, white matter tracts connecting the NAc and Amygdala could be reliably detected in individual participants. (**D**) No significant between group differences were observed for the density of the NAc-Amygdala tracts, in both cohorts (Primary cohort: $M_{ASD} = 4.36 \times 10^{-6}$, $SD_{ASD} = 3.92 \times 10^{-6}$, $M_{TD} = 4.46 \times 10^{-6}$, $SD_{TD} = 2.24 \times 10^{-6}$, $t(46) = -0.11$, $P = 0.91$, BF = 0.29, *Cohen's d* = −0.03; Replication Cohort: $M_{ASD} = 4.04 \times 10^{-6}$, $SD_{ASD} = 1.70 \times 10^{-6}$, $M_{TD} = 4.10 \times 10^{-6}$, $SD_{TD} = 2.02 \times 10^{-6}$, $t(32) = -0.10$, $P = 0.92$, BF = 0.33, *Cohen's d* = −0.03). (**E**) There was no significant association between the density of the NAc- Amygdala tracts and social interaction deficits, as measured by ADI-R social interaction subscale, in both cohorts (Primary Cohort: r_s (22) = −0.19, $P = 0.39$, BF = 0.50; Replication Cohort: $r_s(15) = -0.12$, $P = 0.67$, BF = 0.46).

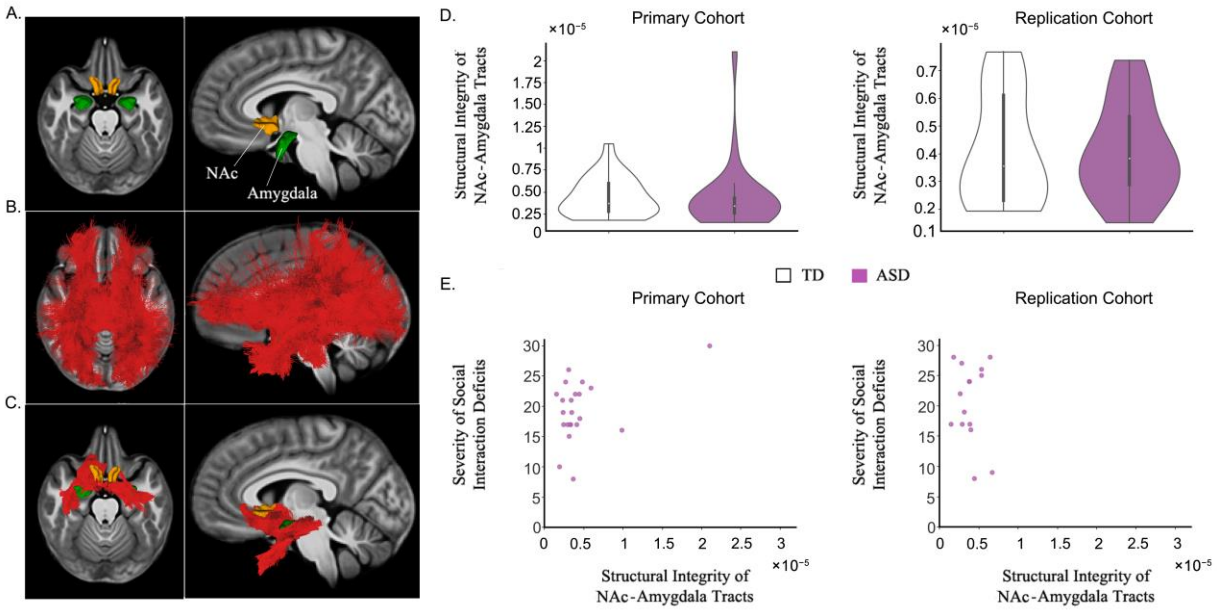

Figure 2. **Aberrant functional connectivity in mesolimbic reward pathway for social stimuli in children with ASD – reduced sample based on a more stringent movement criterion (ASD = 13; TD = 13).** (**A**) Each participant viewed social stimuli (faces)and non-social stimuli (scenes). (**B**) Functional connectivity between the NAc and VTA during face relative to scene processing was disrupted in ASD. In contrast to their TD peers, children with ASD showed lower functional connectivity between the NAc and the VTA when viewing faces compared to scenes (M_{ASD} = −0.46, SD_{ASD} = 0.60, M_{TD} = 0.16, SD_{TD} = 0.85, $t(24)$ = −2.16, P = 0.03, BF = 1.88, *Cohen's d* = −0.85).

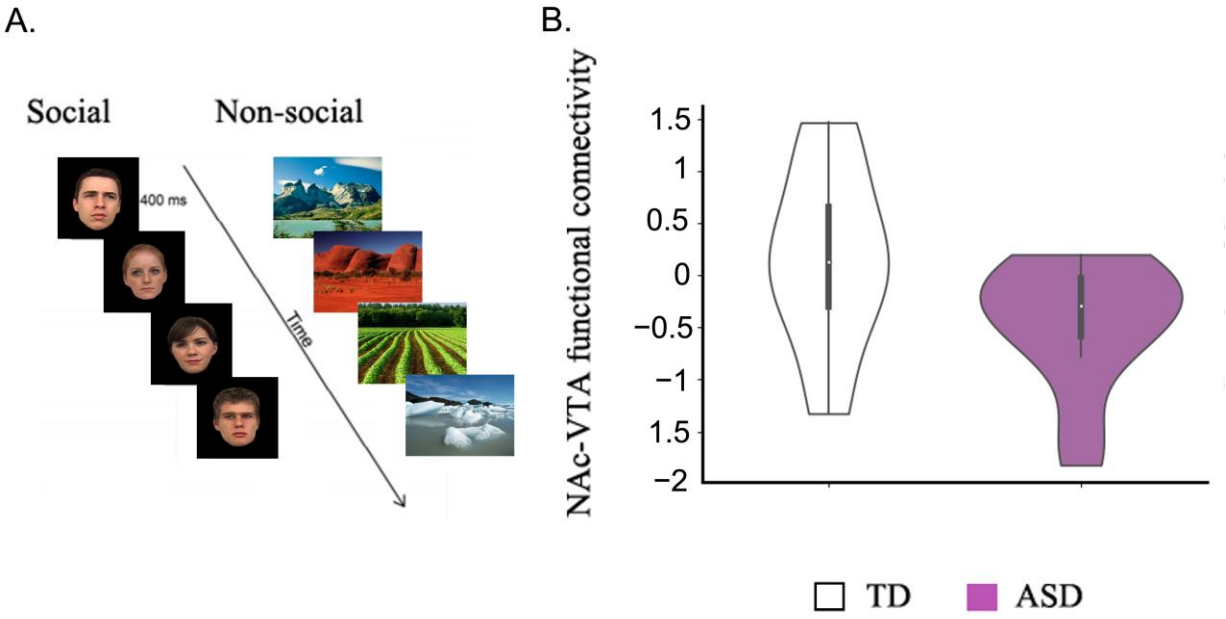

Tables

Table 1. Participant demographics - HARDI

	Primary Cohort (HARDI)[a]			**Replication Cohort (HARDI)[b]**		
	ASD (*n* = 24)	**TD (*n* = 24)**	*P*	**ASD (*n* = 17)**	**TD (*n* = 17)**	*P*
Age	10.62 ± 0.28	10.39 ± 0.25	0.54	10.60 ± 0.30	10.57 ± 0.34	0.94
Gender	23 M: 1 F	24 M: 0 F	0.83	15 M: 2 F	15 M: 2 F	1
IQ	113.67 ± 3.90	121.29 ± 3.65	0.16	107.59 ± 3.88	116.82 ± 2.76	0.06
ADI-R Social Interaction	19.00 ± 1.48			20.47 ± 1.66		
ADI-R Communication and Language	15.93 ± 1.28			16.40 ± 1.24		
ADI-R Restricted Repetitive Behaviors	5.47 ± 0.81			6.53 ± 0.65		
ADOS Social	10.14 ± 0.82			11.13 ± 0.83		
ADOS Restricted Repetitive Behaviors	2.64 ± 0.43			1.93 ± 0.33		

[a]In Primary Cohort (HARDI), ADI scores were not available for 2 participants and ADOS scores were not available for 4 participants.
[b]In Replication Cohort (HARDI), ADI and ADOS scores were not available for 2 participants.

Table 2. Participant demographics - fMRI

	Primary Cohort (HARDI)		
	ASD (*n* = 16)	**TD (*n* = 20)**	*P*
Age	10.82 ± 0.39	10.46 ± 0.29	0.46
Gender	13 M: 3 F	20 M: 0 F	0.08
IQ	115.94 ± 4.80	124.80 ± 4.04	0.17
ADI-R Social Interaction	21.56 ± 0.87		
ADI-R Communication and Language	16.88 ± 1.25		
ADI-R Restricted Repetitive Behaviors	5.50 ± 0.74		
ADOS Social	9.38 ± 0.71		
ADOS Restricted Repetitive Behaviors	2.50 ± 0.33		

Table 3. Summary of HARDI quality measures

	Primary Cohort (HARDI)			**Replication Cohort (HARDI)**		
	ASD (*n* = 24)	**TD (*n* = 24)**	*P*	**ASD (*n* = 17)**	**TD (*n* = 17)**	*P*
Translation	1.29 ± 0.11	1.31 ± 0.11	0.90	2.72 ± 0.14	2.61 ± 0.11	0.56
Rotation	0.03 ± 0.01	0.03 ± 0.01	0.55	0.02 ± 0.001	0.02 ± 0.001	0.38
% Bad Slices	0.48 ± 0.14	0.35 ± 0.13	0.50	0.21 ± 0.06	0.24 ± 0.07	0.76
Dropout score	1.15 ± 0.02	1.14 ± 0.03	0.98	1.13 ± 0.03	1.14 ± 0.03	0.70

Table 4. Summary of fMRI quality measures

	Primary Cohort (fMRI)			Primary Cohort (fMRI – low motion reduced sample)		
	ASD (*n* = 16)	**TD (*n* = 20)**	*P*	**ASD (*n* = 13)**	**TD (*n* = 13)**	*P*
Mean FD	0.32 ± 0.06	0.32 ± 0.09	0.88	0.23 ± 0.04	0.13 ± 0.02	0.07
Range x	1.83 ± 0.26	2.77 ± 0.80	0.22	1.72 ± 0.30	1.84 ± 0.82	0.22
Range y	3.86 ± 0.85	5.45 ± 1.74	0.37	3.82 ± 1.02	1.69 ± 0.47	0.37
Range z	6.25 ± 1.05	5.54 ± 1.15	0.75	5.56 ± 1.02	3.18 ± 0.67	0.75
Range roll	2.71 ± 0.88	3.30 ± 0.78	0.54	1.77 ± 0.30	2.17 ± 0.57	0.54
Range pitch	5.47 ± 1.14	7.14 ± 1.78	0.39	4.34 ± 0.90	3.05 ± 0.72	0.39
Range yaw	2.33 ± 0.84	2.56 ± 0.98	0.80	1.33 ± 0.20	2.16 ± 1.42	0.80
AROMA %var removed	34 ± 6	32 ± 5	0.68	35 ± 7	37 ± 7	0.68

Table 5: Relationship between structural connectivity and ASD symptom severity: Multivariate analysis (Primary Cohort). In the primary cohort, multivariate sparse linear regression with cross-validation analysis revealed that structural deficits in mesolimbic reward pathway are uniquely associated with social interaction impairments in children with ASD.

	β	z	*P*
ADI-R Social Interaction	−0.618	−2.895	**0.007**
ADI-R Communication and Language	0.417	1.416	0.155
ADI-R Restricted Repetitive Behaviors	−0.283	−1.111	0.234
Age	−0.285	−1.415	0.155
IQ	0.039	0.195	0.820

Table 6: Relationship between structural connectivity and ASD symptom severity: Multivariate analysis (Replication Cohort). In the replication cohort, multivariate sparse linear regression with cross-validation analysis revealed that structural deficits in mesolimbic reward pathway are uniquely associated with social interaction impairments in children with ASD.

	β	z	*P*
ADI-R Social Interaction	−0.625	−2.397	**0.028**
ADI-R Communication and Language	0		
ADI-R Restricted Repetitive Behaviors	0		
Age	0		
IQ	0		

Table 7: Relationship between functional connectivity and ASD symptom severity: Multivariate analysis (Primary Cohort). In the primary cohort, multivariate regression with cross-validation analysis revealed aberrant functional connectivity in mesolimbic reward pathway for social stimuli are uniquely associated with social interaction impairments in children with ASD.

	β	z	*P*
ADI-R Social Interaction	−0.615	−2.890	**0.004**
ADI-R Communication and Language	−0.144	−0.571	0.641
ADI-R Restricted Repetitive Behaviors	−0.279	−1.384	0.180
Age	−0.464	−1.900	0.219
IQ	−0.381	−1.859	0.070

Table 8: Relationship between functional connectivity and ASD symptom severity: Multivariate analysis (Primary Cohort – reduced sample). In the primary cohort (reduced fMRI sample; *n* = 13 children with ASD), multivariate regression with cross-validation analysis revealed aberrant functional connectivity in mesolimbic reward pathway for social stimuli are uniquely associated with social interaction impairments in children with ASD

	β	z	*P*
ADI-R Social Interaction	−0.653	−2.484	**0.015**
ADI-R Communication and Language	0		
ADI-R Restricted Repetitive Behaviors	−0.300	−1.158	0.268
Age	−0.365	−1.257	0.253
IQ	−0.311	−1.135	0.311

References

Avants BB, Tustison NJ, Song G, Cook PA, Klein A, Gee JC. A reproducible evaluation of ANTs similarity metric performance in brain image registration. NeuroImage 2011; 54(3): 2033-44.

Benner T, van der Kouwe AJ, Sorensen AG. Diffusion imaging with prospective motion correction and reacquisition. Magn Reson Med 2011; 66(1): 154-67.

Delgado MR, Nystrom LE, Fissell C, Noll DC, Fiez JA. Tracking the hemodynamic responses to reward and punishment in the striatum. J Neurophysiol 2000; 84(6): 3072-7.

Eapen M, Zald DH, Gatenby JC, Ding Z, Gore JC. Using high-resolution MR imaging at 7T to evaluate the anatomy of the midbrain dopaminergic system. AJNR Am J Neuroradiol 2011; 32(4): 688-94.

Fischl B, Salat DH, Busa E, Albert M, Dieterich M, Haselgrove C, *et al.* Whole brain segmentation: automated labeling of neuroanatomical structures in the human brain. Neuron 2002; 33(3): 341-55.

Glover GH, Law CS. Spiral-in/out BOLD fMRI for increased SNR and reduced susceptibility artifacts. Magnetic Resonance in Medicine 2001; 46(3): 515-22.

Koldewyn K, Yendiki A, Weigelt S, Gweon H, Julian J, Richardson H, *et al.* Differences in the right inferior longitudinal fasciculus but no general disruption of white matter tracts in children with autism spectrum disorder. Proceedings of the National Academy of Sciences of the United States of America 2014; 111(5): 1981-6.

Lainhart JE. Advances in autism neuroimaging research for the clinician and geneticist. Am J Med Genet C Semin Med Genet 2006; 142C(1): 33-9.

Lord C, Risi S, Lambrecht L, Cook EH, Jr., Leventhal BL, DiLavore PC, *et al.* The autism diagnostic observation schedule-generic: a standard measure of social and communication deficits associated with the spectrum of autism. J Autism Dev Disord 2000; 30(3): 205-23.

Luyster R, Gotham K, Guthrie W, Coffing M, Petrak R, Pierce K, *et al.* The Autism Diagnostic Observation Schedule-toddler module: a new module of a standardized diagnostic measure for autism spectrum disorders. J Autism Dev Disord 2009; 39(9): 1305-20.

McLaren DG, Ries ML, Xu G, Johnson SC. A generalized form of context-dependent psychophysiological interactions (gPPI): a comparison to standard approaches. NeuroImage 2012; 61(4): 1277-86.

Parkes L, Fulcher B, Yucel M, Fornito A. An evaluation of the efficacy, reliability, and sensitivity of motion correction strategies for resting-state functional MRI. bioRxiv 2017.

Pruim RH, Mennes M, van Rooij D, Llera A, Buitelaar JK, Beckmann CF. ICA-AROMA: A robust ICA-based strategy for removing motion artifacts from fMRI data. NeuroImage 2015; 112: 267-77.

Rohde GK, Barnett AS, Basser PJ, Marenco S, Pierpaoli C. Comprehensive approach for correction of motion and distortion in diffusion-weighted MRI. Magn Reson Med 2004; 51(1): 103-14.

The Psychological C. Wechsler Abbreviated Scale of Intelligence. San Antonio: Harcourt Brace & Co.; 1999.

Tibshirani R. Regression Shrinkage and Selection via the Lasso. Journal of the Royal Statistical Society Series B (Methodological) 1996; 58(1): 267-88.

Tournier JD, Calamante F, Connelly A. MRtrix: Diffusion tractography in crossing fiber regions. International Journal of Imaging Systems and Technology 2012; 22(1): 53-66.

Tournier JDC F, Connely A. Improved probabilistic streamlines tractography by 2nd order integration over fibre orientation distributions. International Society for Magnetic Resonance Medicine; 2010; Stockholm, Sweden; 2010. p. 1670.

Van Essen DC, Ugurbil K, Auerbach E, Barch D, Behrens TE, Bucholz R, *et al.* The Human Connectome Project: a data acquisition perspective. NeuroImage 2012; 62(4): 2222-31.

Wechsler D. The Wechsler Individual Achievement Test — Second Edition (WIAT-II): The Psychological Corporation 2001.

Yendiki A, Koldewyn K, Kakunoori S, Kanwisher N, Fischl B. Spurious group differences due to head motion in a diffusion MRI study. NeuroImage 2014; 88: 79-90.